Electronic Supplementary Material (ESI) for ChemComm.

Supporting Information

Hematite nanorod arrays top-decorated with MIL-101 layer for photoelectrochemical water oxidation

Huali Wang, Xuan He,* Weixin Li, Hui Chen, Wei Fang, Pan Tian, Zhaohui Huang, Lei Zhao.*

The State Key Laboratory of Refractories and Metallurgy, Wuhan University of Science & Technology, Wuhan 430081, P.R. China.

Corresponding Author:

E-mail: xuan.he@wust.edu.cn; zhaolei@wust.edu.cn

Present address: No. 947, Heping Avenue, Qingshan District, Wuhan, Hubei Province, China

EXPERIMENTAL SECTION

Preparation of Fe_2O_3 Nanorod Arrays

All regents were analytically pure and used without subsequent treatment. The Fe_2O_3 nanorod arrays on FTO was synthesized based on a modified reported hydrothermal process.[1] In a typical procedure, the FTO glass was washed by sonication in acetone, methanol, and deionized water, separately. Ferric chloride hexahydrate ($FeCl_3$ $6H_2O$, 3 mmoL), urea (H_2NCONH_2, 3 mmoL) were dissolved in 50 mL of deionized water, and then the homogeneous mixture was transferred into a Teflon-lined autoclave, followed by placing the as-cleaned FTO glass with conductive side up, and kept at 95 ℃ for 5 h in an oven. After cooling, the product was carefully taken out and rinsed with ethanol and deionized water for several times and annealed at 550 ℃ for 2 h with a heating rate of 10 ℃/min tunder ambient conditions, followed by heated to 750 ℃ with a heating rate of 20 ℃/min and kept for 15 min to achieve the crystal transition from β-FeOOH to α-Fe_2O_3.

Preparation of MIL-101 Powders

The MIL-101 was prepared following the previous literature.[2] $FeCl_3$ $6H_2O$ and H_2BDC were mixed at molar ratio about 2: 1 in 50 mL DMF. Subsequently, mixed solution was poured into a Teflon-lined autoclave and stayed at 110 ℃ for 24 h. After cooled down to room temperature, the as-synthesized powders were washed with DMF and ethanol repeatedly and then dried in a vacuum oven to obtain MIL-101 powders.

Preparation of Fe_2O_3/MIL-101 Heterojunction

The Fe_2O_3/MIL-101 heterojunction was prepared *via* a facile CVD process. An

open quartz boat filled with 1, 4-benzenedicarboxylic acid (1, 4-BDC, 9 mmoL) was placed into the middle of a horizontal quartz tube, in the terminal of which was settled the pre-fabricated Fe_2O_3 film. Two filter plugs were placed at both ends of the pipe and then argon (Ar) was replenished and evacuated for three cycles to pure the gas path. Afterwards, the pipe was heated up to 400 ℃ with a constant rate of 5 ℃/min and kept for 30 min, 60 min and 90 min, respectively, with Ar carrier pumped in continuously. The obtained Fe_2O_3/MIL-101 was immersed by N, N-dimethyl-formamide (DMF), ethanol and deionized water in sequent and then dried at 60 ℃. The samples were severally noted as F/M-30, F/M-60 and F/M-90 for short.

CHARATERIZATION

The powder X-ray diffraction (XRD) patterns were operated on a Philips X'Pert Pro diffractometer by Ni-filtered Cu Kα radiation (λ = 0.154056 nm) with Bragg diffraction angle between 5 °- 90 °. The Fourier Transform Raman spectra were collected using a Thermo Fisher DXR2xi 5225 microscope with a DXR 532 nm laser. X-ray photoelectron spectroscopy (XPS) measurements were studied by a VG Multilab 2000 instrument (Thermo Electron Corporation) with Al Kα radiation. The field emission scanning electron microscope (SEM) images were observed on a FEI Company Novo 400 device with a voltage of 18 kV. The energy dispersive X-ray (EDX) element mappings were scanned on a Thermo Electron Corporation Noran 623M-3SUT spectroscope. The transmission electron microscopy (TEM) images were characterized by a JEOL JEM-1400Plus at an accelerating voltage of 120 kV. UV-visible diffuse

reflectance (UV-Vis) spectroscopy was recorded using a Shimadzu UV-2600 spectrophotometer with a transparent FTO glass subtracting the background. The steady-state photoluminescence (PL) emission spectra were tested on Shimadzu RF-6000v with an excitation wavelength of 268 nm, and time-resolved photoluminescence (PL) spectroscopy was conducted by FLS980 Spectrometer (Edinburgh Instruments Ltd.) at room temperature. The fluorescence decay plots were measured employing a pulsed excitation laser of 370 nm and detected on a high-speed red.

Photo-electrochemical Measurements

PEC measurements were carried on CHI 660E electrochemical workstation equipped with a standard three-electrode configuration, adopting the obtained photoanode as a work electrode, the Pt foil as a counter electrode and the Ag/AgCl electrode in 3 M KCl as a reference electrode. Fe_2O_3 and Fe_2O_3/MIL-101 films were carefully scraped into photoanodes with a geometric area of 0.5 cm × 0.5 cm by a squeegee blade. A fresh 1 M NaOH (pH = 13.7) solution purified by nitrogen for 30 min was applied as the electrolyte medium. A 500 W Xenon lamp equipped with an AM 1.5 G filter (Zolix) was utilized as the light source with an irradiance intensity of 100 mW cm^{-2} calibrated by an NREL-standard Si solar cell. The photo-electrochemical impedance spectroscopy (PEIS) was tested with an AC amplitude of 10 mV and frequency range of 1 Hz to 100 KHz. The incident photon-to-current conversion efficiency (IPCE) was tested by the Zennium C-IMPS system (Zahner, TLS-03) with wavelength from 365 nm to 800 nm. Mott-Schottky (M-S) analysis was recorded on a

Zennium Photo-electrochemical instrument (Zahner IM6 and PP211, Germany), in which the AC amplitude is 10 mV and the frequency is 1 KHz. All the above PEC performance was completed under front-side irradiation at a bias of 0.3 V *vs.* Ag/AgCl, which is about 1.3 V *vs.* RHE according to the following equation: $E_{RHE} = E_{Ag/AgCl} + 0.059 \times pH + 0.197$ at 25 ℃.[1]

Calculation of Applied bias photo-to-current efficiency

Applied bias photon-to-current conversion efficiency (ABPE) is converted through the equation: $\eta_{ABPE} = \frac{J \times (1.23 - V_{app})}{I_0}$, where J represents the real-time measured photocurrent density, V_{app} is the applied bias voltage and I_0 means incident light power density (100 mW cm^{-2}). [3]

Calculation of Incident Photon-to-current Conversion Efficiency

The incident photon-to-current conversion efficiency (IPCE) is calculated by $IPCE_{(\lambda)} = \frac{j_{ph}\ (mA \cdot cm^{-2}) * 1240\ (V \cdot nm)}{P_{mono}\ (mW \cdot cm^{-2}) * \lambda\ (nm)}$, in which j_{ph} represents the photocurrent density with the wavelength λ and the power intensity Pmono of incident light.[4]

Calculation of the Electrochemical Active Surface Area

The electrochemical active surface area (ECSA) is obtained by testing cyclic voltammetry curves at different scanning rates in the non-Faradaic region of 0.9 - 1.2 V. According to plotting charging current difference ($\Delta I = I_a - I_c$) at 1.05 V against the scan rates, the electric double layer capacitance (C_{dl}) is acquired, which is the half of the slope of the fitted line. The ECSA can be calculated from C_{dl} according to the following: $ECSA = C_{dl} / C_s$, in which C_s means the specific capacitance of the sample.[5]

Supplemental Graphics

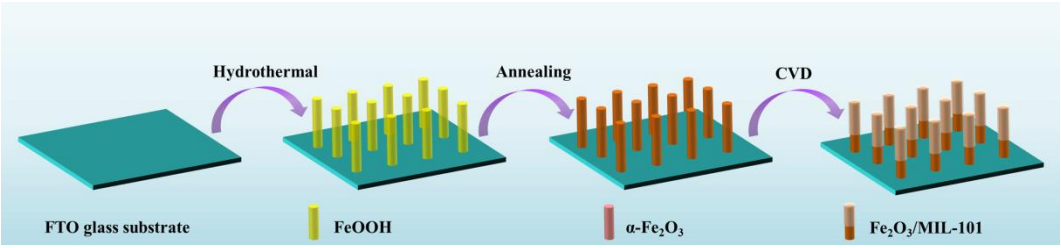

Scheme S1. The step-by-step synthetic procedure for Fe_2O_3/MIL-101 heterojunction.

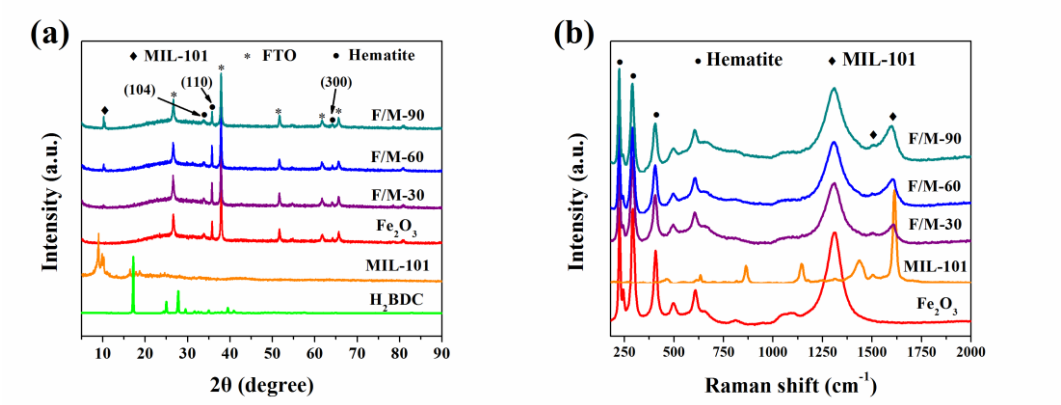

Figure S1. (a) XRD patterns of Fe_2O_3, MIL-101，H_2BDC and Fe_2O_3/MIL-101 heterojunctions; (b) Raman spectra of Fe_2O_3, MIL-101 and Fe_2O_3/MIL-101 heterojunctions.

The characteristic peaks at 220 cm^{-1}, 285 cm^{-1}, 400 cm^{-1} confirm the existence of hematite phase as illustrated by Raman spectra in **Fig. S1b**.[6] The characteristic peaks at 1614 cm^{-1} are ascribed to the C-O stretching vibration resulting from organic linkers in MIL-101.[7] Furthermore, the intensity of peak at 1614 cm^{-1} increase with the holding time of CVD process since that of F/M-90 is higher than others, which is strictly accordance with that of XRD.

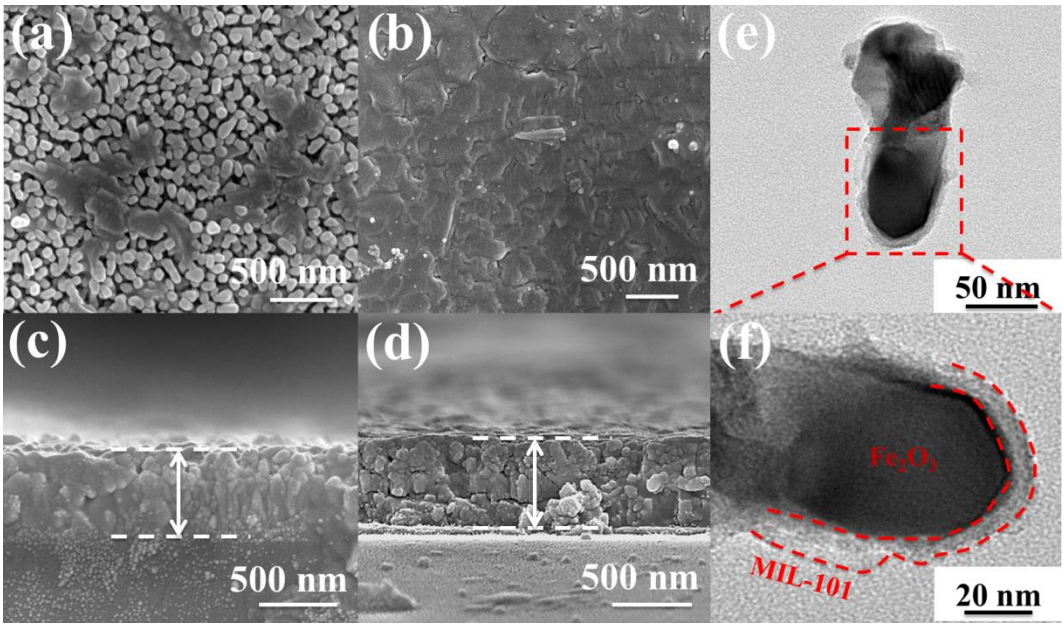

Fig. S2 (a) Top-view and (c) cross-section-view SEM images of the F/M-30, (b) Top-view and (d) cross-section-view SEM images of the F/M-90, (e, f) TEM images of the F/M-90 with different magnification.

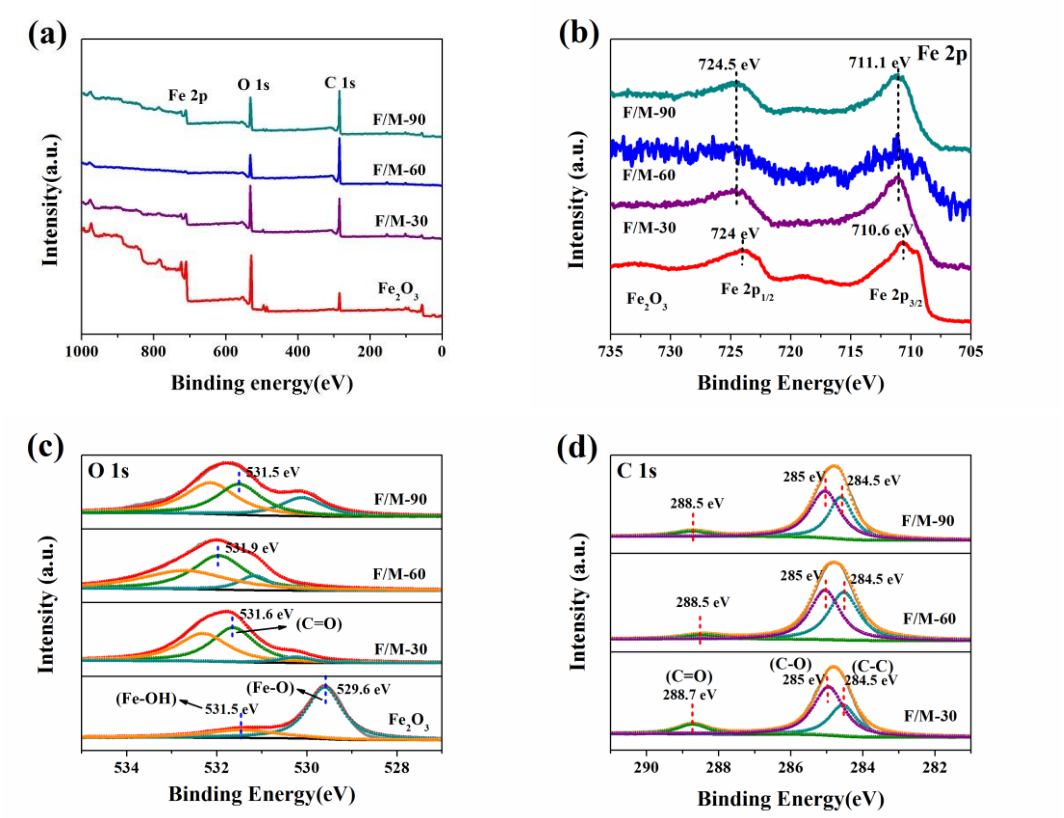

Figure S3. (a) Survey scan; (b) Fe 2p XPS spectra; (c) O 1s XPS spectra of Fe_2O_3, F/M-30, F/M-60 and F/M-90, respectively; (d) C 1s XPS spectra of F/M-30, F/M-60 and F/M-90.

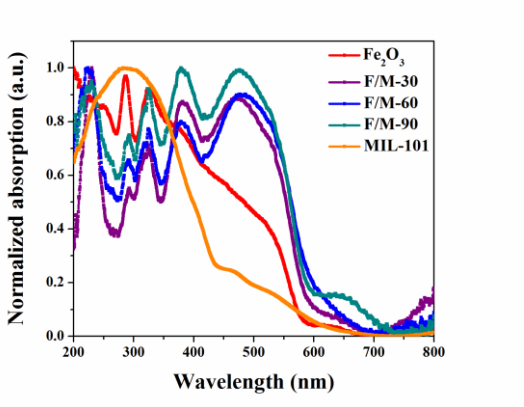

Figure S4. UV−vis diffuse reflectance spectra of MIL-101, Fe_2O_3 and Fe_2O_3/MIL-101 photoanodes.

Optical performance of samples is evaluated by UV-Vis spectra. As demonstrated in **Fig. S4**, a broad absorption ranging in 200 - 580 nm is exhibited for Fe_2O_3 film, while the absorption features of Fe_2O_3/MIL-101 samples are found to be similar to that. Moreover, the optical absorption of heterojunctions in the visible light region is enhanced and the optical absorption edge is slightly red shifted, revealing that the thin MIL-101 layer impact positive influence on optical absorption of the Fe_2O_3 photoanode.

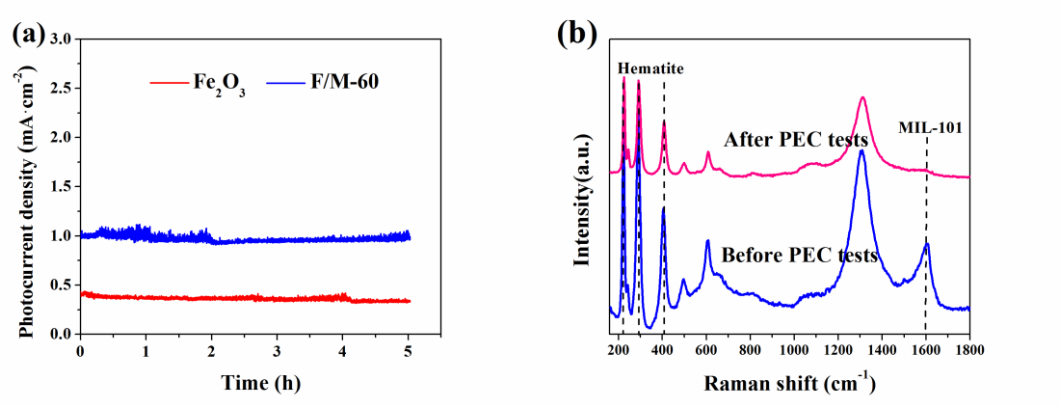

Figure S5. (a) Stability of Fe_2O_3 and F/M-60 photoanodes under light illumination at 1.3 V vs. RHE, (b) Raman spectra of F/M-60 before and after PEC tests.

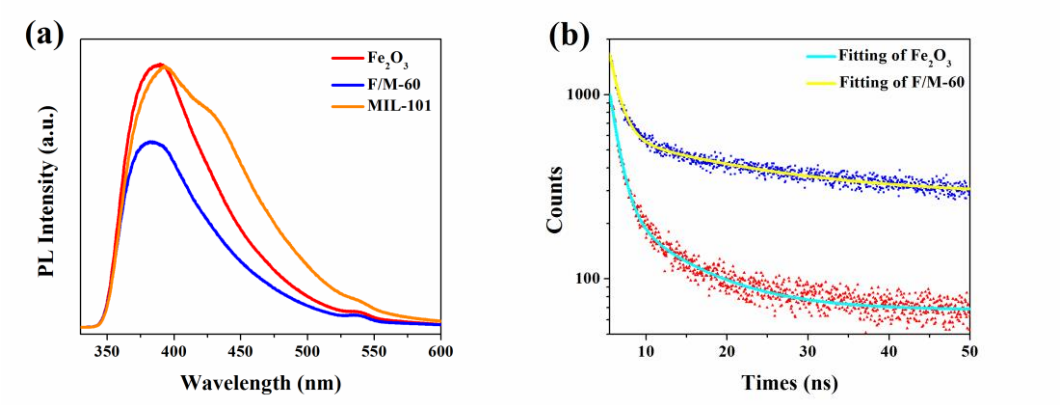

Figure S6. (a) Steady-state PL spectra of Fe_2O_3 NAs, MIL-101 and F/M-60; (b) time-resolved PL spectra of Fe_2O_3 and F/M-60.

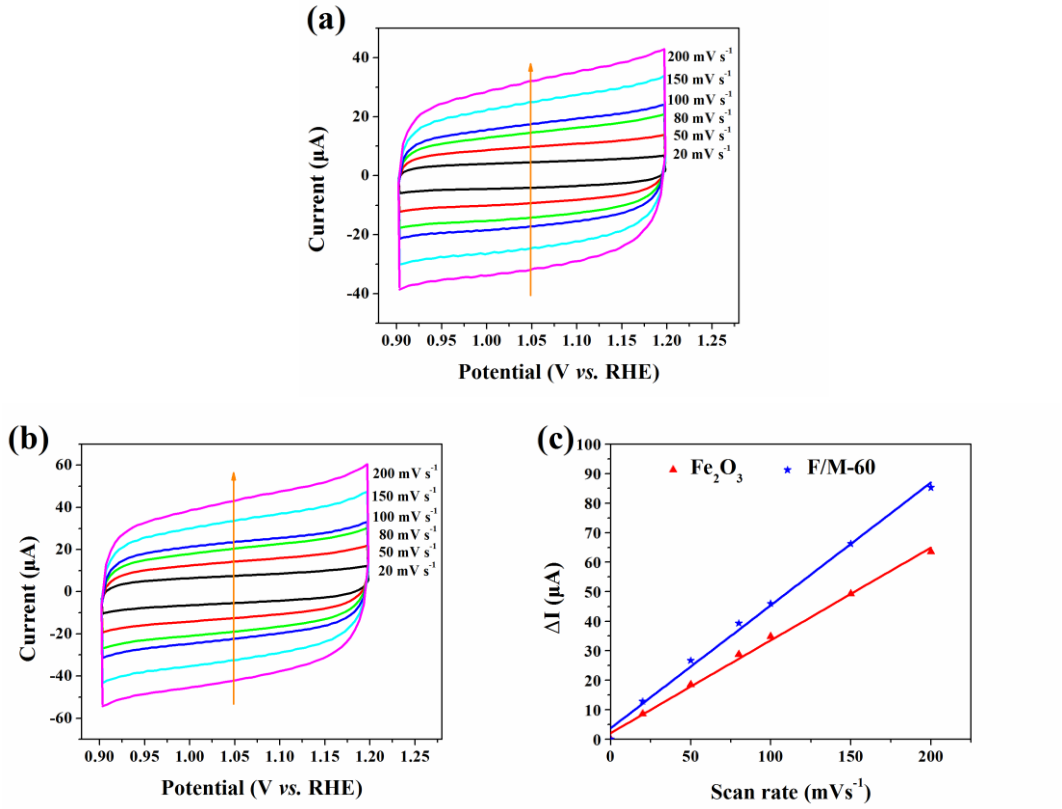

Figure S7. CV curves measured in a non-Faradaic region of 0.9 - 1.2 V at various scan rates for (a) Fe_2O_3, (b) F/M-60, (c) Charging current differences ($\Delta I = Ia - Ic$) against scan rate for Fe_2O_3 and F/M-60, respectively.

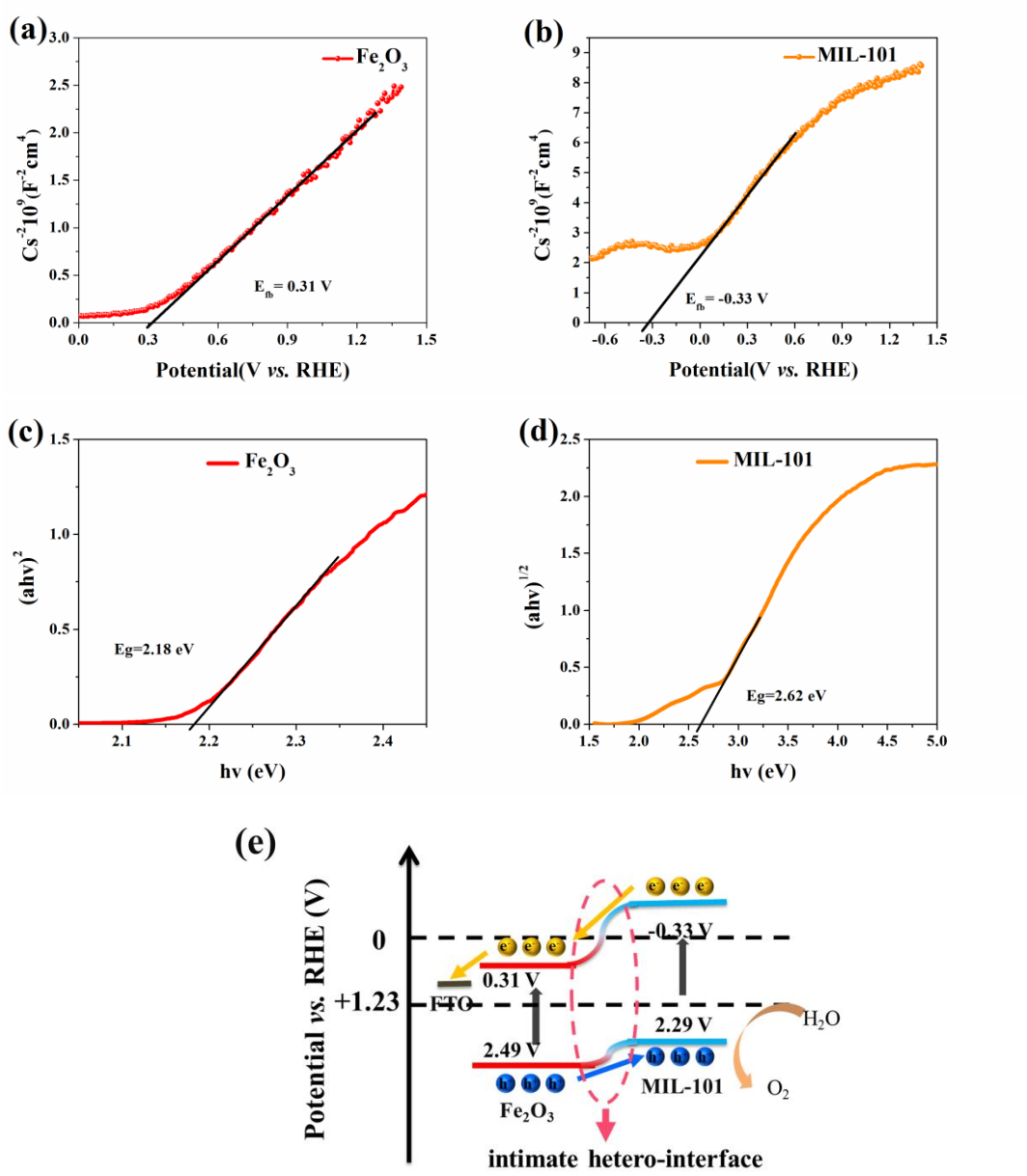

Fig S8. Mott-Schottky plots of of (a) Fe_2O_3 and (b) MIL-101; Tauc plots of (c) Fe_2O_3 and (d) MIL-101, (e) energy band structure diagram of Fe_2O_3/MIL-101.

Mott-Schottky measurement is taken under the dark condition to analyze the band edges of Fe_2O_3 and MIL-101. From **Fig. S8(a, b)**, the flat band potential (Efb) of Fe_2O_3 and MIL-101 are respectively 0.31 V and -0.33 V *vs.* RHE, which can be approximately considered as the bottom of the conductive band (CB).[8] The energy bandgaps of Fe_2O_3 and MIL-101 are individually determined to be 2.18 eV (**Fig. S8c**)

and 2.62 eV (**Fig. S8d**) with Tauc's plots: $(\alpha h\nu) = A(h\nu - Eg)^{n/2}$, in which n is corresponding to 1 for MIL-101 (direct-bandgap) and 4 for Fe_2O_3 (indirect-bandgap).[7, 9] The corresponding valance band (VB) positions are calculated apart to be 2.49 V for the former and 2.29 V for the latter. As presented in **Fig. S8e**, the CB position of MIL-101 is more negative comparing to that of Fe_2O_3, which is in favor of photogenerated electrons to migrate to Fe_2O_3. Furthermore, relatively lower position of VB of MIL-101 prefers to attract holes as well to result in a type-Ⅱ heterojunction constituted in samples of Fe_2O_3/MIL-101 series for efficient separation of electron-hole pairs.

Table S1. The atomic ratio of carbon in Fe_2O_3/MIL-101.

Sample	F/M-30	F/M-60	F/M-90
C (A %)	63.97 %	71.43 %	80.99 %

Table S2. Dynamics of Picosecond-Resolved Fluorescence Transients of Fe_2O_3 and F/M-60.

Sample	τ_1 (ns)	τ_2 (ns)	A_1%	A_2%	χ^2	τ_A(ns)
Fe_2O_3	1.1698	1.2708	38.82%	61.18%	1.037	1.23
F/M-60	1.2708	18.0995	19.93%	80.07%	1.122	17.8

The average lifetimes (τ_A) are calculated by the following equation: $\tau = (A_1\tau_1^2 + A_2\tau_2^2) / (A_1\tau_1 + A_2\tau_2)$, which are 1.23 ns for Fe_2O_3 and 17.8 ns for F/M-60. The significantly prolonged τ_A means the long-term survival of charges with a low annihitation possibility, leading to the efficient charge separation and surface reactions.[3, 10, 11]

Table S3. The corresponding values of R_1 and R_2 calculated from the EIS measurements.

Sample	R_1 (Ω)	R_2 (Ω)
Fe_2O_3	3.201	4207
F/M-60	4.545	1577

Table S4. Comparison of the photocurrent density with reported literatures at different voltages.

Photoanodes	**Fabrication method**	**Photocurrent density**	**References**
AuPt/Fe_2O_3	Spin-coating process	0.06 mA cm^{-2} (1.23 V *vs.* RHE)	12
$Ni(OH)_2/Fe_2O_3$	Hydrothermal method	0.55 mA cm^{-2} (1.5 V *vs.* RHE)	13
α-Fe_2O_3/NiOOH	Photo/electro-deposition	0.625 mA cm^{-2} (1.23 V *vs.* RHE)	14
Co_3O_4/Fe_2O_3	Plasma-assisted route	0.66 mA cm^{-2} (1.5 V *vs.* RHE)	15
α-Fe_2O_3 NRs/Sb_2S_3	Hydrothermal method	~0.7 mA cm^{-2} (1.375 V *vs.* RHE)	16
α-Fe_2O_3/TiO_2	Aqueous chemical growth	0.5 mA cm^{-2} (2 V *vs.* RHE)	17
NiO_x/Fe_2O_3	Photodeposited	0.8 mA•cm^{-2} (1.5 V vs. RHE)	18
Fe_2O_3/MIL-101	CVD	1.0 mA cm^{-2} (1.3 V *vs.* RHE)	This work

Reference

1. Y.-H. Wu, W.-R. Guo, M. Mishra, Y.-C. Huang, J.-K. Chang and T.-C. Lee, *ACS Applied Nano Materials*, 2018, **1**, 3145-3154.
2. D. Wang, R. Huang, W. Liu, D. Sun and Z. Li, *Acs Catalysis*, 2014, **4**.
3. T. Rui, S. Zhou, L. Zhang and L. Yin, *Advanced Functional Materials*, 2018, 1706154.
4. J. Zhou, A. Zhou, L. Shu, M. C. Liu, Y. Dou and J. R. Li, *Applied Catalysis B Environmental*, 2018, **226**, 421-428.
5. X. Li, S. Liu, K. Fan, Z. Liu, B. Song and J. Yu, *Advanced Energy Materials*, 2018, 1800101.
6. H. Xia, C. Hong, B. Li, B. Zhao, Z. Lin, M. Zheng, S. V. Savilov and S. M. Aldoshin, *Advanced Functional Materials*, 2015, **25**, 627-635.
7. Z. Zhang, X. Li, B. Liu, Q. Zhao and G. Chen, *Rsc Advances*, 2016, **6**, 4289-4295.
8. J. Fu, B. Zhu, C. Jiang, B. Cheng, W. You and J. Yu, *Small*, 2017, **13**.
9. Y. Li, H. Xu, S. Ouyang, D. Lu, X. Wang, D. Wang and J. Ye, *Journal of Materials Chemistry A*, 2016, **4**, 2943-2950.
10. J. Zhou, A. Zhou, L. Shu, M. C. Liu, Y. Dou and J. R. Li, *Applied Catalysis B: Environmental*.
11. F. Ning, M. Shao, S. Xu, Y. Fu, R. Zhang, M. Wei, D. G. Evans and X. Duan, *Energy & Environmental Science*, 2016, **9**, 2633-2643.
12. B. Chen, W. Fan, B. Mao, H. Shen and W. Shi, *Dalton Transactions*, 2017.
13. Q. Li, J. Bian, N. Zhang and D. H. Ng, *Electrochimica Acta*, 2015, **155**, 383-390.
14. F. Malara, A. Minguzzi, M. Marelli, S. Morandi, R. Psaro, V. Dal Santo and A. Naldoni, *ACS catalysis*, 2015, **5**, 5292-5300.
15. G. Carraro, C. Maccato, A. Gasparotto, K. Kaunisto, C. Sada and D. Barreca, *Plasma Processes and Polymers*, 2016, **13**, 191-200.
16. D. Chen, Z. Liu, M. Zhou, P. Wu and J. Wei, *Journal of Alloys and Compounds*, 2018, **742**, 918-927.
17. R. Venkatkarthick, D. J. Davidson, S. Ravichandran, S. Vasudevan and G. Sozhan,

Materials Chemistry and Physics, 2017, **199**, 249-256.

18. F. Malara, F. Fabbri, M. Marelli and A. Naldoni, *ACS Catalysis*, 2016, **6**, 3619-3628.